Non-intrusive reduced order modeling of multi-phase flow in porous media using the POD-RBF method

D. Xiao[a,c], F. Fang[a,*], C.C. Pain[a], I.M. Navon[b], P. Salinas[a]

[a] *Applied Modelling and Computation Group, Department of Earth Science and Engineering,Imperial College London, Prince Consort Road, London, SW7 2BP, UK.URL:* `http://amcg.ese.imperial.ac.uk`
[b] *Department of Scientific Computing, Florida State University,Tallahassee, FL, 32306-4120, USA*
[c] *State Key Laboratory of Geological Processes and Mineral Resources, China University of Geosciences, Wuhan, 430074, China*

Abstract

A novel non-intrusive reduced order model (ROM) based on a radial basis function (RBF) method and proper orthogonal decomposition (POD) has been developed for multiphase flows in porous media. The advantage of this method is that it is generic and non-intrusive, that is, it does not require modifications to the source code, as it is independent of the governing equations and discretization of the system. The novelties introduced in this work are in (1) the use of the RBF interpolation method to represent solutions of the time-dependent POD equations; (2) the first attempt of applying such a non-intrusive reduced order method to multiphase porous media simulation, and (3) the first implementation of the non-intrusive ROM under the framework of a complex unstructured mesh control volume finite element (CVFEM) multiphase model.

The capability of this new POD-RBF ROM has been numerically illustrated in two multiphase flow simulations in porous media: a two material layer case and a low permeability domain embedded in a high permeability domain case. By comparing the results of the POD-RBF ROM against the solutions obtained from the high fidelity full model, it is shown that this model can result in a large reduction in the CPU computation cost (by a factor of 2500) while much of the details of multiphase flow in porous media are captured.

Keywords: RBF, POD, porous media, reduced order modelling, finite element

1. Introduction

The simulations of multiphase flows in porous media are very important and have a wide range of applications, from groundwater production to radioactive waster and the extraction of oil and gas from the subsurface. However, the application of multiphase modelling in industry is not only computationally intensive, but also often suffers from

*Corresponding author
Email address: `f.fang@imperial.ac.uk` (F. Fang)

significant uncertainties in the controlling parameters used as inputs when predicting the performance. In this paper a new non-intrusive reduced order modelling technique is presented aiming to address this issue by presenting an approach which is capable of resolving complex multiphase porous media flows while avoiding the high computational cost.

The reduced order modelling technique has been shown to be a powerful capability of representing the large dynamical systems using only a few number of reduced order basis functions. The multiphase porous media model can be projected into a reduced space, therefore, the computational efficiency can be enhanced by several orders of magnitude if we use hyper-reduction techniques. Among the model reduction methods, the POD approach is the most widely used. This method extracts the most energetic parts of the system through snapshots method, and then constructs optimal basis functions. The POD method and its variants have been successfully applied to numerous research fields. In geophysical fluid dynamics it is referred to as empirical orthogonal functions (EOF) [1, 2], in signal analysis and pattern recognition it is termed as Karhunen-Love method [3] and in statistics it is called the principal component analysis (PCA) method [4]. The POD technique has also been applied to ocean models[5, 6, 7, 8], air pollution modeling [9], mesh optimization [10] and the shallow water equations. This includes the work of Stefanescu et al.[11, 12], Daescu and Navon [13], Altaf et al. [14], Chen *et al.* [15, 16] and Du et al. [17].

POD in combination with the Galerkin projection method is an effective method for deriving a reduced order model (ROM). However, this method suffers from numerical instability [18]. Various methods have been proposed to overcome or improving the stability issue of the POD/Galerkin projection method, including nonlinear Petrov−Galerkin [7, 19], regularisation [20], subgrid-scale modelling, calibration [21, 22] and *F*ourier expansion [23]. Another issue that arises in the ROMs is the efficient treatment of non-linear terms in the partial differential equations (PDEs). A number of efficient non-linear treatment methods have been presented, for example, the empirical interpolation method (EIM)[24] and its discrete version discrete empirical interpolation method (DEIM) [25], residual DEIM (RDEIM) [6], Petrov−Galerkin projection method [21], Gauss−Newton with approximated tensors method [26] and the quadratic expansion method [27, 28].

However, these methods are still dependent on the governing equations of the full physical system. In most cases the source code describing the full physical system has to be modified in order to form the reduced order model. These modifications can be complex, especially in legacy codes, or may not be possible if the source code is not available (*e.g.* in some commercial software) [29]. To circumvent these shortcomings, more recently, non-intrusive methods have been introduced into ROMs, which do not require the knowledge of the governing equations and the original source code [29]. Chen et al. proposed a non-intrusive model reduction method based on blackbox stencil interpolation method and machine learning method [29]. Audouze et al. proposed a non-intrusive reduced order modelling approach for nonlinear parametrized time-dependent PDEs based on a two-level POD method. This method is verified and validated using Burgers equation and convection-diffusion-reaction problems [30, 31]. Walton et al. proposed a non-intrusive reduced order technique for unsteady fluid flow using radial basis function interpolation and POD [32].

Recently, reduced order methods (*e.g*, POD, POD/DEIM, trajectory piecewise linearisation and bilinear approximation techniques) have been applied to reservoir modelling [33, 34, 35, 36, 37, 38, 39, 40]. Heijn *et al.* [33] and Cardoso *et al.* [34, 35] first developed POD reduced order models for reservoir simulation. Chaturantabut *et al.* [36], Yang *et al.* [37] and Yoon *et al.* [38] further introduced DEIM into model reduction for non-linear flows [36]. Again, these reduced order methods are intrusive and equations/codes dependent. There are very few studies in non-intrusive reduced order modelling in porous media flow simulation. Klie first proposed a non-intrusive model reduction approach based on a three-layer neural network combined with POD and DEIM to predict the production of oil and gas reservoirs [40], where the RBF neural network is used for developing learning functions from input-output relationships. In this work, we used RBF as an interpolation method for constructing the time-dependent POD ROM.

The current paper applies, for the first time, a non-intrusive POD-RBF method to generate reduced order model for multiphase flows in porous media. This has been implemented under the framework of a unstructured mesh finite element porous media flow model. The novelty of this work lies in the use of the RBF interpolation method combined with POD to represent the solution of the multiphase porous media equations on the reduced spaces. In this approach, solutions to the full fidelity model are recorded (as a sequence of snapshots), and from these snapshots POD bases are generated that optimally represent the porous media flow problem. The RBF interpolation method is then used to form a hypersurface interpolation function that approximates the time-dependent ROM. After obtaining the hypersurface, the solution of ROM at the current time levels can be calculated by inputting POD coefficients of earlier time levels into this hypersurface. The capabilities of results from the new POD-RBF multiphase flow model have been assessed by two multiphase flow test cases in porous media: a two material layer case and a low permeability domain embedded in a high permeability domain case. Comparisons between the high fidelity full model and this non-intrusive ROM are made to investigate the accuracy of the POD-RBF formulation.

The structure of the paper is as follows: section 2 presents the governing equations of the multiphase porous media flows; section 3 presents the reduced order modelling method using POD-RBF method; section 4 illustrates the methodology derived by means of two numerical examples. The illustration consists of two test problems where a two material layer test case and a low permeability domain embedded in a high permeability domain case are resolved. Finally in section 5, the conclusion is presented.

2. Governing equations

The governing equations used in the underlying multiphase model are given in this section. The darcy's law for immiscible multiphase flow in porous media has the form:

$$\mathbf{q}_\alpha = -\frac{\mathcal{K}_{r_\alpha}}{\mu_\alpha}\mathbf{K}\left(\nabla p_\alpha - \mathbf{s}_{u\alpha}\right), \tag{1}$$

where $\mathbf{q}_\alpha$ is the α^{th} phase Darcy velocity. The $\mathcal{K}_{r_\alpha}$ is the relative permeability of the α^{th} phase, and it is a function that is denoted by $\mathcal{K}_{r_\alpha}(S_\alpha)$ corresponding to the phase saturation variable S_α. p_α is the pressure of the α^{th} phase, which may include capillary pressure. $\mathbf{K}$ is the absolute permeability tensor of the porous medium. μ_α and $\mathbf{s}_{u_\alpha}$ are the phase dynamic viscosity and source term respectively, which may include gravity.

A saturation-weighted Darcy velocity is introduced into the equation (1) and defined as

$$\mathbf{v}_\alpha = \frac{\mathbf{q}_\alpha}{S_\alpha}, \tag{2}$$

then equation (1) can be rewritten as follows:

$$\mathbf{u}_\alpha = \underline{\underline{\sigma}}_\alpha \mathbf{v}_\alpha = -\nabla p_\alpha + \mathbf{s}_{u\alpha}, \quad \underline{\underline{\sigma}}_\alpha = \mu_\alpha S_\alpha (\mathcal{K}_{r_\alpha}\mathbf{K})^{-1} \tag{3}$$

where $\mathbf{u}_\alpha$ denotes the force per unit volume, which is defined as $\underline{\underline{\sigma}}_\alpha \mathbf{v}_\alpha$ and used as a prognostic variable in this approach. The $\underline{\underline{\sigma}}_\alpha$ represents the implicit linearisation of the viscous frictional forces.

The saturation equation can be written as:

$$\phi \frac{\partial S_\alpha}{\partial t} + \nabla \cdot (\mathbf{v}_\alpha S_\alpha) = s_{cty,\alpha}, \tag{4}$$

where ϕ denotes the porosity. The t is time and $s_{cty,\alpha}$ is a source term of the α^{th} phase. Finally, equation (4) is bounded by the constraint:

$$\sum_{\alpha=1}^{N_\alpha} S_\alpha = 1, \tag{5}$$

where N_α denotes the number of phases.

2.1. Discretisation of the governing equations

The discretisation of the above equations (1)-(5) at time level n can be written in a general form:

$$\mathbf{A}_v^n \mathbf{v}^n = \mathbf{s}_v^n, \quad \mathbf{A}_p^n \mathbf{p}^n = \mathbf{s}_p^n, \quad \mathbf{A}_S^n \mathbf{S}^n = \mathbf{s}_S^n \tag{6}$$

where $\mathbf{v}^n = (\mathbf{v}_1^n, \ldots, \mathbf{v}_\alpha^n, \ldots, \mathbf{v}_{N_\alpha}^n)^T$, and $\mathbf{v}_\alpha^n = (v_{\alpha,1}, \ldots, v_{\alpha,\mathcal{N}})^T$, $\mathbf{S}_\alpha^n = (S_{\alpha,1}, \ldots, S_{\alpha,\mathcal{N}})^T$, $\mathbf{p}^n = (P_{\alpha,1}, \ldots, P_{\alpha,\mathcal{N}})^T$ and $\mathcal{N}$ is the number of nodes.

3. Non-intrusive reduced order model based on a POD-RBF method

3.1. Proper Orthogonal Decomposition (POD) formulation

POD is a numerical technique used to find a set of optimal basis functions from the snapshots of solutions obtained from the original model. The optimal POD basis functions are then used to formulate a reduced dynamical system that contains the main features of the flow. Due to the optimality of convergence in terms of kinetic energy of the POD basis functions, dominant components of a large dimensional process can be captured with only a small number of bases *e.g.*, 10 – 100.

In POD formulation, the variable vectors $\mathbf{v}^n$, $\mathbf{p}^n$ and $\mathbf{S}^n$ at time level n can be expressed:

$$\mathbf{v}^n = \overline{\mathbf{v}} + \Phi_v^T \mathbf{v}_r^n, \quad \mathbf{p}^n = \overline{\mathbf{p}} + \Phi_p^T \mathbf{p}_r^n, \quad \mathbf{S}^n = \overline{\mathbf{S}} + \Phi_S^T \mathbf{S}_r^n, \tag{7}$$

where $\overline{\mathbf{v}}$, $\overline{\mathbf{p}}$ and $\overline{\mathbf{S}}$ are the mean of the ensemble of snapshots for the variables $\mathbf{v}^n$, $\mathbf{p}^n$ and $\mathbf{S}^n$ respectively, $\Phi_v = (\Phi_{v,1}, \ldots, \Phi_{v,M})$, $\Phi_p = (\Phi_{p,1}, \ldots, \Phi_{p,M})$, $\Phi_S = (\Phi_{S,1}, \ldots, \Phi_{S,M})$ are the POD bases for $\mathbf{v}^n$, $\mathbf{p}^n$ and $\mathbf{S}^n$ respectively, which are extracted through truncated singular value decomposition, and M is the number of POD bases used in the POD model, $\mathbf{v}_r^n = (\mathbf{v}_{r,1}^n, \ldots, \mathbf{v}_{r,j}^n, \ldots, \mathbf{v}_{r,M}^n)^T$, $\mathbf{p}_r^n = (\mathbf{p}_{r,1}^n, \ldots, \mathbf{p}_{r,j}^n, \ldots, \mathbf{p}_{r,M}^n)^T$ and $\mathbf{S}_r^n = (\mathbf{S}_{r,1}^n, \ldots, \mathbf{S}_{r,j}^n, \ldots, \mathbf{S}_{r,M}^n)^T$ denote the reduced variable vectors (POD coefficients) at time level n. Projecting equation (6) onto the reduced space, yields:

$$\Phi_v^T \mathbf{A}_v^n \Phi_v \mathbf{v}^n = \mathbf{s}_v^n, \quad \Phi_p^T \mathbf{A}_p^n \Phi_p \mathbf{p}^n = \mathbf{s}_p^n, \quad \Phi_S^T \mathbf{A}_S^n \Phi_S \mathbf{S}^n = \mathbf{s}_S^n \tag{8}$$

The POD ROM for solving the POD coefficients $\mathbf{v}_{r,j}^n$, $\mathbf{p}_{r,j}^n$ and $\mathbf{S}_{r,j}^n$ (where $j \in \{1, 2, \ldots M\}$) at time level n can be written in the general form:

$$\begin{aligned} \mathbf{v}_{r,j}^n &= f_{v,j}(\mathbf{v}_r^{n-1}, \mathbf{p}_r^{n-1}, \mathbf{S}_r^{n-1}), \\ \mathbf{p}_{r,j}^n &= f_{p,j}(\mathbf{v}_r^{n-1}, \mathbf{p}_r^{n-1}, \mathbf{S}_r^{n-1}), \\ \mathbf{S}_{r,j}^n &= f_{S,j}(\mathbf{v}_r^{n-1}, \mathbf{p}_r^{n-1}, \mathbf{S}_r^{n-1}), \end{aligned} \tag{9}$$

subject to the initial condition

$$\mathbf{v}_{r,j}^0 = ((\mathbf{v}_j^0 - \overline{\mathbf{v}}), \Phi_j), \quad \mathbf{p}_{r,j}^0 = ((\mathbf{p}_j^0 - \overline{\mathbf{p}}), \Phi_j), \quad \mathbf{S}_{r,j}^0 = ((\mathbf{S}_j^0 - \overline{\mathbf{S}}), \Phi_j), \tag{10}$$

where $\mathbf{v}_r^{n-1}$, $\mathbf{p}_r^{n-1}$ and $\mathbf{S}_r^{n-1}$ denotes a complete set of POD coefficients for solution fields $\mathbf{v}$, $\mathbf{p}$ and $\mathbf{S}$ at time step $n-1$ ($n \in \{1, 2, \ldots, N_t\}$), N_t is the number of time levels in the computational simulation.

3.2. Radial basis functions interpolation

The Radial basis functions interpolation method constructs function approximations in the form of

$$f(\mathbf{x}) = \sum_{i=1}^{N} w_i \, \phi(\|\mathbf{x} - \mathbf{x}_i\|), \tag{11}$$

where the interpolation function $f(\mathbf{x})$ is represented as a linear combination of N radial basis functions(ϕ). Each RBF is associated with a different center x_i, and weighted by a coefficient w_i. $\|\mathbf{x} - \mathbf{x}_i\|$ is a scalar distance defined by the L_2 norm.

In the RBF interpolation problem, the weight coefficients w_i are determined by ensuring that the interpolation function values $f(\mathbf{x})$ will match the given data y exactly. This is achieved by enforcing $f(\mathbf{x}) = y$, which produces a linear equation

$$Aw = y, \tag{12}$$

where

$$A = \begin{bmatrix} \phi(\|x_1 - x_1\|_2) & \phi(\|x_1 - x_2\|_2) & \cdots \phi(\|x_1 - x_n\|_2) \\ \phi(\|x_2 - x_1\|_2) & \phi(\|x_2 - x_2\|_2) & \cdots \phi(\|x_2 - x_n\|_2) \\ \vdots & \vdots & \vdots \\ \phi(\|x_n - x_1\|_2) & \phi(\|x_n - x_2\|_2) & \cdots \phi(\|x_n - x_n\|_2) \end{bmatrix}, \tag{13}$$

$$w = [w_1, w_2, ..., w_n]^T, y = [y_1, y_2, ..., y_n]^T \tag{14}$$

The weight coefficients w_j are then determined by solving the linear system (12) $Aw = y$. How to define an appropriate RBF ϕ is also important, a number of most well-known choices for ϕ are listed in table 1, where $r \geqslant 0$ is a radius and $\sigma > 0$ is a shape parameter. The standard RBFs have two major types: Infinitely smooth RBFs

Table 1: some well-known Radial Basis Functions

Type	Name of functions	Definition
Type I	Gaussian (GA)	$\phi(r) = e^{-(r/\sigma)^2}$
	Multi-Quadratic	$\phi(r) = \sqrt{r^2 + \sigma^2}$
	Inverse Multi-Quadratic	$\phi(r) = \frac{1}{\sqrt{r^2+\sigma^2}}$
	Inverse Quadratic	$\phi(r) = \frac{1}{r^2+\sigma^2}$
Type II	Thin Plate Spline	$\phi(r) = r^2 log\, r$

and Infinitely smooth (except at centres) RBFs. [41, 42].

Type I: Infinitely smooth RBFs are infinitely differentiable and dependent on the shape parameter σ, *e.g.* Gaussian (GA), Multi-Quadratic (MQ), Inverse Quadratic (IQ) and Inverse Multi-quadratic (IMQ) in table 1.

Type II: Infinitely smooth (except at centres) RBFs are independent on shape parameter and are not differentiable infinitely, *e.g.* thin plate spline in table 1.

The infinitely smooth RBFs ensure the matrices A in equation 12 non-singular and symmetric [43]. The basis functions of Infinitely smooth (except at centres) RBFs are comparatively less accurate than that of Infinitely smooth RBFs [41].

In the following section, the implementation of POD-RBF method is described. An advantage of RBF interpolation should be point out here is that this method is meshless, which means the distribution of sample nodes are not necessarily to be regular.

3.3. Implementation of the non-intrusive POD model based on the RBF method

In this work, the radial basis function (RBF) interpolation has been used to construct the POD ROM in (9). The advantage of the POD-RBF method over the traditional Galerkin projection POD models is its non-intrusiveness, i.e. it does not require the knowledge of the governing equations and the original code.

By applying the RBF method, a set of multidimensional functions $f^n_{v,j}$, $f^n_{p,j}$ and $f^n_{S,j}$ for each POD coefficient $v^n_{r,j}$, $p^n_{r,j}$ and $S^n_{r,j}$ ($j \in \{1, 2, \ldots, M\}$) may be approximately

represented by the hypersurface interpolation function below:

$$\begin{aligned} v^n_{r,j} &= f_{v,j}(\mathbf{v}^{n-1}_r, \mathbf{p}^{n-1}_r, \mathbf{S}^{n-1}_r) = \sum_{i=1}^{N} w_{v,i,j} * \phi(r_i), \\ p^n_{r,j} &= f_{p,j}(\mathbf{v}^{n-1}_r, \mathbf{p}^{n-1}_r, \mathbf{S}^{n-1}_r) = \sum_{i=1}^{N} w_{p,i,j} * \phi(r_i), \\ S^{\,n}_{r,j} &= f_{S,j}(\mathbf{v}^{n-1}_r, \mathbf{p}^{n-1}_r, \mathbf{S}^{n-1}_r) = \sum_{i=1}^{N} w_{S,i,j} * \phi(r_i), \end{aligned} \tag{15}$$

where $\phi(r_i)$ is the radial basis function whose values depend on the distance from a collection data point, $(\hat{\mathbf{v}}_{r,i}, \hat{\mathbf{p}}_{r,i}, \hat{\mathbf{S}}_{r,i})$ (where $i \in 1, 2, \ldots, N$) and weighted by $w_{v,i}$, $w_{v,i}$ and $w_{v,i}$. In this work, the multiquadratic functions are chosen:

$$\phi(r_i) = \sqrt{r_i^2 + \sigma^2} = \sqrt{\left\|(\mathbf{v}^{n-1}_r, \mathbf{p}^{n-1}_r, \mathbf{S}^{n-1}_r) - (\hat{\mathbf{v}}_{r,i}, \hat{\mathbf{p}}_{r,i}, \hat{\mathbf{S}}_{r,i})\right\|^2 + \sigma^2}, \tag{16}$$

where $r_i = \left\|(\mathbf{v}^{n-1}_r, \mathbf{p}^{n-1}_r, \mathbf{S}^{n-1}_r) - (\hat{\mathbf{v}}_{r,i}, \hat{\mathbf{p}}_{r,i}, \hat{\mathbf{S}}_{r,i})\right\|$ is a radius or the distance defined by the L_2 norm, $\sigma > 0$ is a shape parameter).

The weighting coefficients $w_{v,i}$, $w_{v,i}$ and $w_{v,i}$ are determined so as to ensure that the interpolation function values at the collection data point $(\hat{\mathbf{v}}_{r,k}, \hat{\mathbf{p}}_{r,k}, \hat{\mathbf{S}}_{r,k})$ match the given data $f_{v,k}$, $f_{p,k}$ and $f_{S,k}$. This can be expressed by,

$$A\mathbf{w}_{v,i} = \mathbf{f}_{v,i}, \quad A\mathbf{w}_{p,i} = \mathbf{f}_{p,i}, \quad A\mathbf{w}_{S,i} = \mathbf{f}_{S,i}, \quad i \in \{1, 2, \ldots, N\}, \tag{17}$$

where

- $\mathbf{w}_{v,i} = (w_{v,i,k})^T_{k=1,\ldots,N}$, $\mathbf{w}_{p,i} = (w_{p,i,k})^T_{k=1,\ldots,N}$ and $\mathbf{w}_{S,i} = (w_{S,i,k})^T_{k=1,\ldots,N}$,
- $\mathbf{f}_{v,i} = (w_{v,i,k})^T_{k=1,\ldots,N}$, $\mathbf{f}_{p,i} = (w_{p,i,k})^T_{k=1,\ldots,N}$ and $\mathbf{f}_{S,i} = (w_{S,i,k})^T_{k=1,\ldots,N}$,
- A is the interpolation matrix of elements $A_{k,l} = \phi(\left\|(\hat{\mathbf{v}}_{r,k}, \hat{\mathbf{p}}_{r,k}, \hat{\mathbf{S}}_{r,k}) - (\hat{\mathbf{v}}_{r,l}, \hat{\mathbf{p}}_{r,l}, \hat{\mathbf{S}}_{r,l})\right\|)$,
- $k, l \in \{1, 2, \ldots, N\}$, N is the number of data points.

The coefficients $w^{n-1}_{v,i} = (w_{v,i,j})_{j=1,\ldots,N}$, $w^{n-1}_{p,i} = (w_{p,i,j})_{j=1,\ldots,N}$ and $w^{n-1}_{S,i} = (w_{S,i,j})_{j=1,\ldots,N}$ are then determined by solving the linear system (17).

3.4. Summary of POD-RBF reduced order model

Algorithm 1: POD-RBF reduced order modelling

(1) **Offline calculation:** Construct the POD-RBF reduced order model

(a) POD bases

i. Generate the snapshots at time level $n = 1, \ldots, N_t$ by solving the full model (6);

ii. Construct the POD bases Φ_v, Φ_p and Φ_S using the SVD method;

(b) Construct a set of interpolation functions

i. Calculate the functional values $f_{v,i,k}$, $f_{p,i,k}$ and $f_{S,i,k}$ at the data point $(\hat{\mathbf{v}}_{r,k}, \hat{\mathbf{p}}_{r,k}, \hat{\mathbf{S}}_{r,k})$ through the solution from the full models, where $k \in \{1, 2, \ldots N\}$;

ii. Find the weights $\mathbf{w}_{v,i}$, $\mathbf{w}_{p,i}$ and $\mathbf{w}_{S,i}$ by solving (17) such that the interpolation functions $\mathbf{f}_{v,i}$, $\mathbf{f}_{p,i}$ and $\mathbf{f}_{S,i}$ pass through through the data points;

(2) **Online calculation:** The RBF interpolation function in (15) denotes a 3M-dimensional hyper surface. Once a set of interpolation functions $f_{v,j}$, $f_{p,j}$ and $f_{S,j}$ are constructed, they are then used to estimate the j^{th} POD coefficient $v_{r,j}^n$, $p_{r,j}^n$ and $S_{r,j}^n$ at time level n.

Result: Write here the result
Initialization $v_{r,j}^0$, $p_{r,j}^0$ and $S_{r,j}^0$;
for $n = 1$ *to* N_t **do**
  for $j = 1$ *to* M **do**

(i) **Inputs:** a complete set of POD coefficients for solution fields $\mathbf{v}$, $\mathbf{p}$ and $\mathbf{S}$ at time step $n-1$:

$$\mathbf{v}_r^{n-1} = (v_{r,j}^{n-1})_{j=1,\ldots,M}^T, \quad \mathbf{p}^n = (p_{r,j}^{n-1})_{j=1,\ldots,M}^T, \quad \mathbf{S}^n = (S_{r,j}^{n-1})_{j=1,\ldots,M}^T,$$

(ii) **Outputs:** Estimate the POD coefficient $v_{r,j}^n$, $p_{r,j}^n$ and $S_{r,j}^n$ at current time step n using the RBF interpolation (15);

$$\begin{aligned} v_{r,j}^n &= f_{v,j}(\mathbf{v}_r^{n-1}, \mathbf{p}_r^{n-1}, \mathbf{S}_r^{n-1}), \\ p_{r,j}^n &= f_{p,j}(\mathbf{v}_r^{n-1}, \mathbf{p}_r^{n-1}, \mathbf{S}_r^{n-1}), \\ S_{r,j}^n &= f_{S,j}(\mathbf{v}_r^{n-1}, \mathbf{p}_r^{n-1}, \mathbf{S}_r^{n-1}), \end{aligned}$$

  endfor
  Obtain the solution of variables $\mathbf{v}^n$, $\mathbf{p}^n$ and $\mathbf{S}^n$ in (4) by projecting $v_{r,j}^n$, $p_{r,j}^n$ and $S_{r,j}^n$ onto the full space (see (7)).

$$\mathbf{v}^n = \overline{\mathbf{v}} + \Phi_v^T \mathbf{v}_r^n, \quad \mathbf{p}^n = \overline{\mathbf{p}} + \Phi_p^T \mathbf{p}_r^n, \quad \mathbf{S}^n = \overline{\mathbf{S}} + \Phi_S^T \mathbf{S}_r^n,$$

endfor

4. Numerical Examples

4.1. Introduction of an unstructured mesh multiphase fluid model

The POD-RBF reduced order modelling method has been implemented under the framework of an advanced 3D unstructured mesh multiphase fluid model, the Imperial College Finite Element Reservoir Simulator (IC-FERST). A novel control volume finite element method (CVFEM) is used to obtain the high-order fluxes on CV boundaries which are limited to yield bounded fields (*e.g.*, positive saturations). This method is combined with a novel family of FE pairs, originally introduced for geophysical fluid dynamics applications. In particular, the $P2DG - P1DG$ element pair (quadratic discontinuous polynomial FE basis function for velocity ($P2DG$) and linear discontinuous polynomial FE basis function for pressure, $P1DG$), is used to accurately represent sharp saturation changes between heterogeneous domains, see [44, 45].

4.2. General description of test cases

The waterflooding is a widely known technique in oil and gas reservoir engineering. It increases the production from oil reservoirs through injecting water into the reservoir. As illustrated in figure 1, the water is injected into the reservoir to increase the reservoir pressure, the oil is then displaced toward the production well. This phenomenon is also referred to the immiscible displacement in porous media.

In this section, the capability of the POD-RBF ROM has been demonstrated in two porous media flow problems: the two material layer test case and the low permeability domain embedded in a high permeability domain case. These test cases are dimensionless and for simplicity no gravity has been considered. In all cases, the outlet boundary has a dimensionless pressure of 0, the whole domain is initially saturated with the non-wetting phase and the wetting phase at the irreducible saturation. The wetting phase is injected over the inlet boundary with a dimensionless velocity of 1. The viscosity ratio of the phases is 1. The Brooks-Corey model for the relative permeability, with an exponent of 2 and an end-point relative permeability of 1, is considered for both phases. The porosity is homogeneous and equal to 0.2. The immobile fraction of the wetting phase is set to 0.2 and 0.3 for the non-wetting phase.

4.3. Case 1: two material layer test case

The first case for numerical illustration of the method proposed in this paper is a two material layer test case. This problem domain is consist of a rectangle of non-dimensional size 1×0.2. The domain is divided into two identical areas with a permeability of 4 within the top half part and 1 on the bottom half part.

The problem was resolved with a mesh of 984 nodes during the simulation time period $[0, 0.02]$. Fifty snapshots were taken from the pre-computed solution at regularly spaced time intervals $\Delta t = 0.0002$ and from these POD bases are generated for the solution variables v, p, S.

The first 18 POD bases are presented in figure 2. As shown in the figure, the first four POD bases capture most of flow features while the 5^{th}-18^{th} POD bases capture the details of small scale flow structures. Figure 3 shows the singular eigenvalues in order of decreasing magnitude. In general, the more POD bases and snapshots are chosen,

the better the energy is represented. There is a trade-off between the accuracy and the CPU time. In this work, 18 POD bases with 50 snapshots are chosen resulting in 92% of 'energy' being captured.

Figure 4 shows the saturation solutions of the two material layer problem at time instances $t = 0.01$ and $t = 0.02$, as calculated using the full and non-intrusive POD-RBF models. It can be seen that both model solutions are in good agreement with each other. The POD-RBF model performs well in capturing the saturation shock-front.

Figure 5 shows the saturation solution at a particular position (0.026937, 0.16246). It is noted the results from the POD-RBF model using 6 and 12 POD bases become oscillatory after $t = 10$. By increasing the number of POD bases from 6 to 18, the POD-RBF modelling becomes stable and exhibits an overall good agreement with the full modelling.

The ability of the POD-RBF ROM is further highlighted in figure 6, which presents the saturation solution along a line parallel to the x-axies. We can see the POD-RBF model has a large error near the shock-front when using 6 POD bases. This can be significantly improved as the number of POD bases increases. Using 18 POD bases, the error of saturation solutions is decreased by 50% – 97% in comparison to that using only 6 POD bases, and the shock-front is captured well.

To further validate the quality of the POD-RBF ROM, the corresponding error estimation of the POD ROM was carried out in this work. The accuracy of POD-RBF reduced order modelling was assessed. The correlation coefficient of solutions between the full and POD-RBF models is computed for each time step, and is defined for given expected values S^n_{full} and S^n and standard deviations $\sigma_{S^n_{full}}$ and σ_{S^n},

$$corr(S^n_{full}, S^n)^n = \frac{cov(S^n_{full}, S^n)}{\sigma_{S^n_{full}} \sigma_{S^n}} = \frac{E(S^n_{full} - \sigma_{S^n_{full}})(S^n - \sigma_{S^n})}{\sigma_{S^n_{full}} \sigma_{S^n}}. \tag{18}$$

where E denotes mathematical expectation, cov denotes covariance, σ denotes standard deviation. The measured error is given by the root mean square error (RMSE) which is calculated for each time step n by,

$$RMSE^n = \sqrt{\frac{\sum_{i=1}^{N} (S^n_{full,i} - S^n_i)^2}{N}}. \tag{19}$$

In this expression $S^n_{full,i}$ and S^n_i denote the full and POD-RBF model solutions at the node i, respectively, and N represents number of nodes on the full mesh.

The RMSE and correlation coefficient of saturation solutions between the full and POD-RBF models are presented in figure 7. With an increase in the number of POD bases, the RMSE in the saturation results decreases by about 50% while the correlation increases up to 98%.

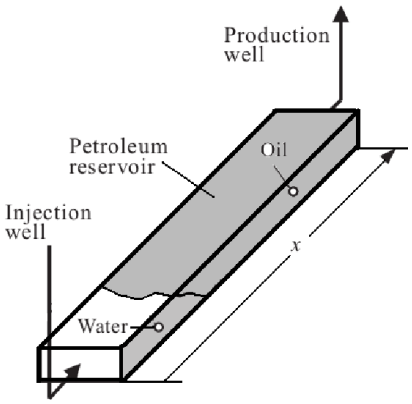

Figure 1: Waterflooding technique for oil production.

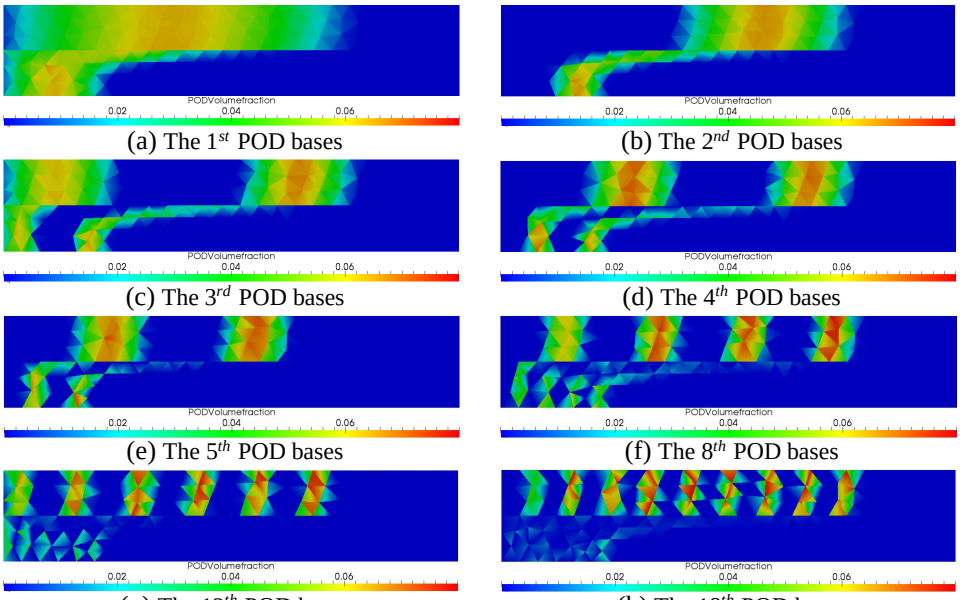

(a) The 1^{st} POD bases (b) The 2^{nd} POD bases

(c) The 3^{rd} POD bases (d) The 4^{th} POD bases

(e) The 5^{th} POD bases (f) The 8^{th} POD bases

(g) The 12^{th} POD bases (h) The 18^{th} POD bases

Figure 2: Case 1: the figures displayed the first 18 the POD bases functions of the 2D two material layer problem.

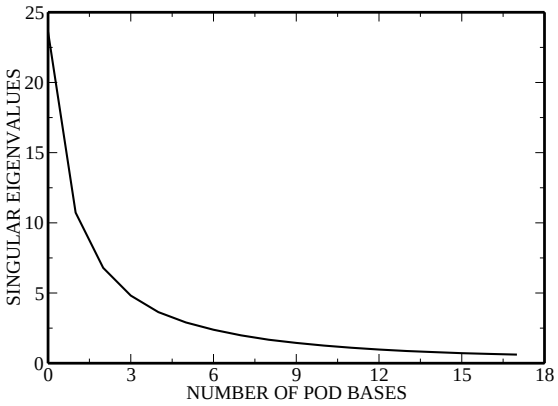

Figure 3: Case 1: the figure shows the singular eigenvalues in order of decreasing magnitude.

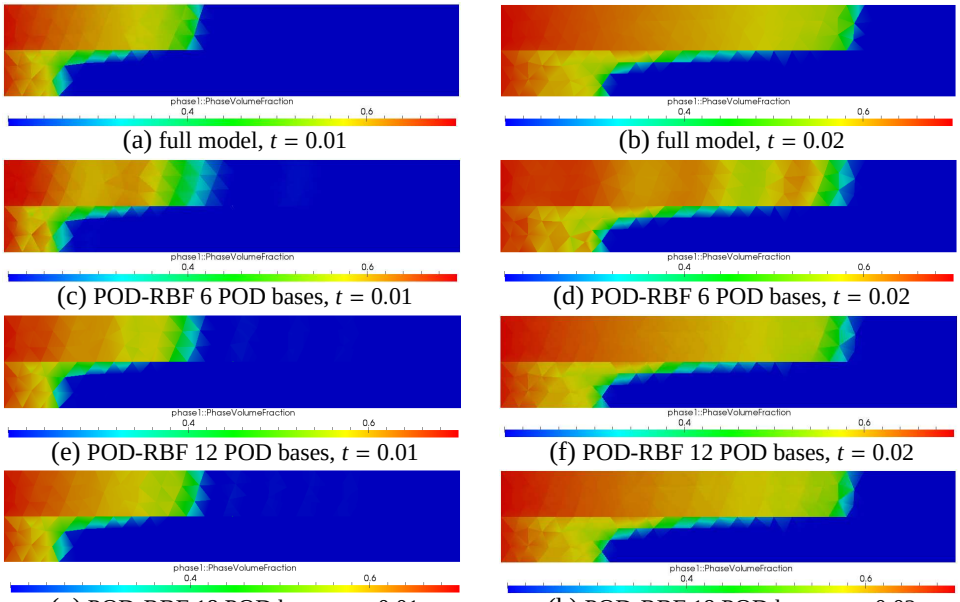

(a) full model, $t = 0.01$ (b) full model, $t = 0.02$

(c) POD-RBF 6 POD bases, $t = 0.01$ (d) POD-RBF 6 POD bases, $t = 0.02$

(e) POD-RBF 12 POD bases, $t = 0.01$ (f) POD-RBF 12 POD bases, $t = 0.02$

(g) POD-RBF 18 POD bases, $t = 0.01$ (h) POD-RBF 18 POD bases, $t = 0.02$

Figure 4: Case 1: the figures displayed above show the saturation solutions of the two material layer problem at time instances 0.01 and 0.02 (where 6, 12 and 18 POD bases are chosen with 50 snapshots). The permeability on the top half part is 4, and the bottom half part is 1.

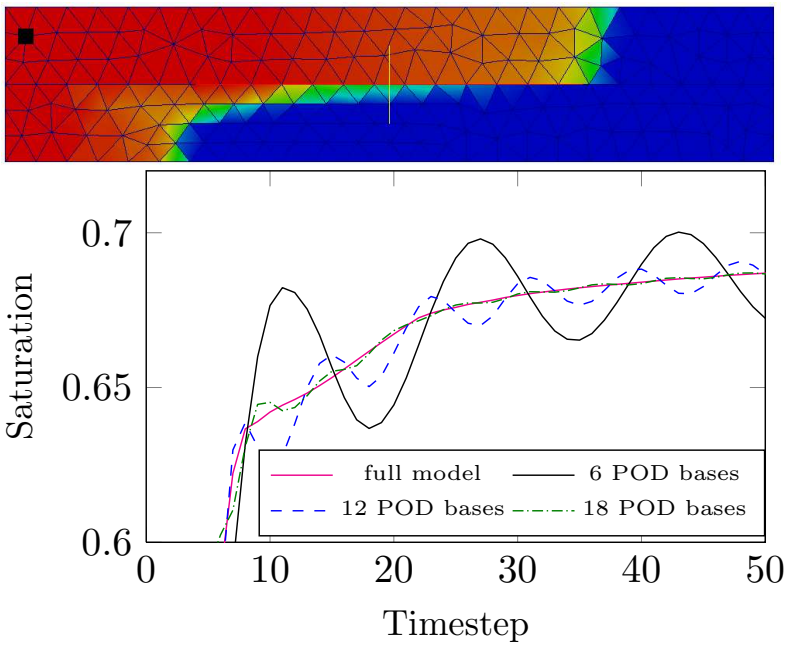

Figure 5: Case 1: the graph shows the solution saturations predicted by the full model and the POD-RBF ROM at a position (0.026937, 0.16246) (where 6, 12 and 18 POD bases are chosen with 50 snapshots)

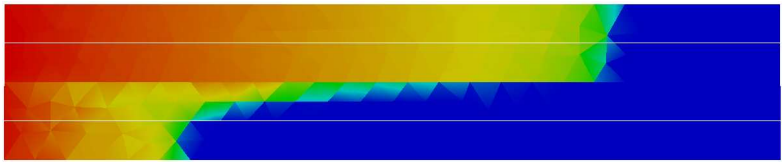

(a) The cross section locations

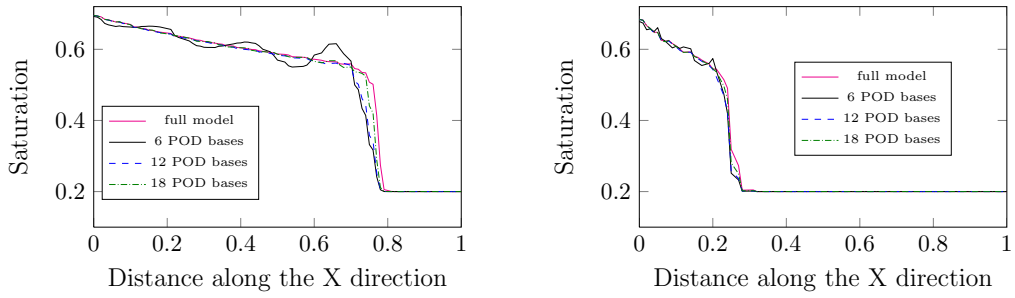

(b) Saturation at the cross section along the top line (c) Saturation at the cross section along the bottom line

Figure 6: Case 1: Saturation along lines parallel to the x axies.

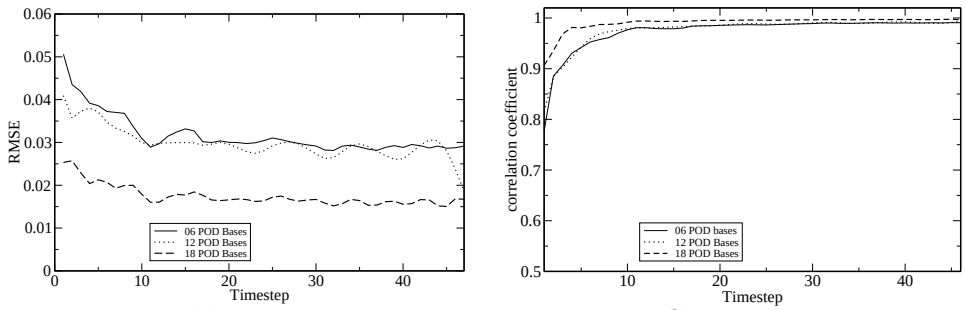

(a) RMSE (b) Correlation

Figure 7: Case 1: The graph shows the RMSE and correlation coefficient of solutions between the full and POD-RBF models.

4.4. Case 2: Low permeability domain embedded in a high permeability domain

The second case is comprised of a low permeability domain embedded in a higher permeability domain. The domain has a non-dimensional size 2×0.5. The low permeability is 0.001 and the high permeability is 1. The full model simulation with a mesh of 1386 nodes was run during the simulation period $[0, 0.1]$ with a time step size of 0.0001. Fifty snapshots of solutions were taken at regularly spaced time intervals $\Delta t = 0.02$ for each solution variable.

Figure 8 shows the first 18 leading POD bases functions of saturation. As shown in the figure, these leading POD bases capture the dominant characteristics of solutions. The POD bases corresponding to small eigenvalues, for example, the 12^{th} and 18^{th} POD bases, contain small scale flow features.

Evaluation of accuracy of the POD model was carried out through comparison of POD solutions with those from the full model. The saturation solutions at time instances 0.05 and 0.1 obtained from the full and POD-RBF models are presented in figure 9. Again, good agreement is observed between the two models. The POD-RBF model is able to capture the complex flow patterns around the block. Both the full and POD-RBF models provide almost identical details of local flows. For example, the separated flow forms downstream of the block.

To further demonstrate the ability of the POD-RBF model, the saturation solution at location $(0.58515, 0.43611)$ is presented in figure 10. It can be seen that the accuracy of solution can be improved by increasing the number of POD bases functions to 18. This is also be shown in figure 11, which illustrates the saturation along lines parallel to the x axies. Again the POD-RBF model performs very well in capturing the saturation shock-front when 18 POD bases are used.

To further assess the accuracy of the POD-RBF model, the absolute error in saturation solutions at time instances 0.05 and 0.1 is plotted in figure 12. It is shown that the error in the POD-RBF solution relative to the high fidelity full model decreases as the number of POD bases is increased.

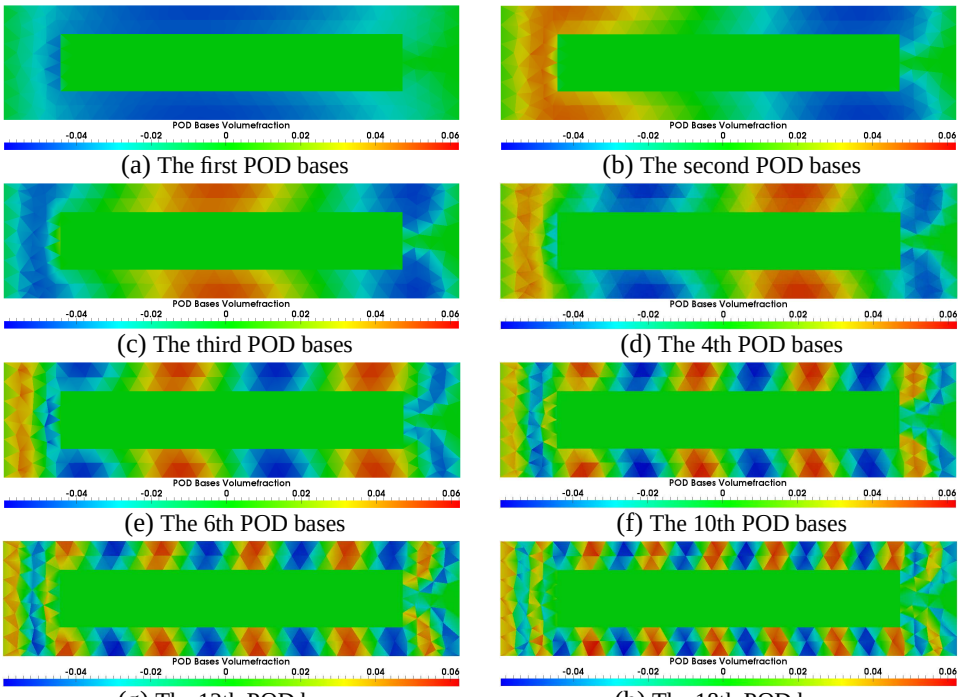

(a) The first POD bases (b) The second POD bases

(c) The third POD bases (d) The 4th POD bases

(e) The 6th POD bases (f) The 10th POD bases

(g) The 12th POD bases (h) The 18th POD bases

Figure 8: Case 2: the figures displayed above shows the leading POD bases functions of saturation. They are the 1^{st}, 2^{nd}, 3^{rd}, 4^{th}, 6^{th}, 10^{th}, 12^{th} and 18^{th} POD bases functions respectively.

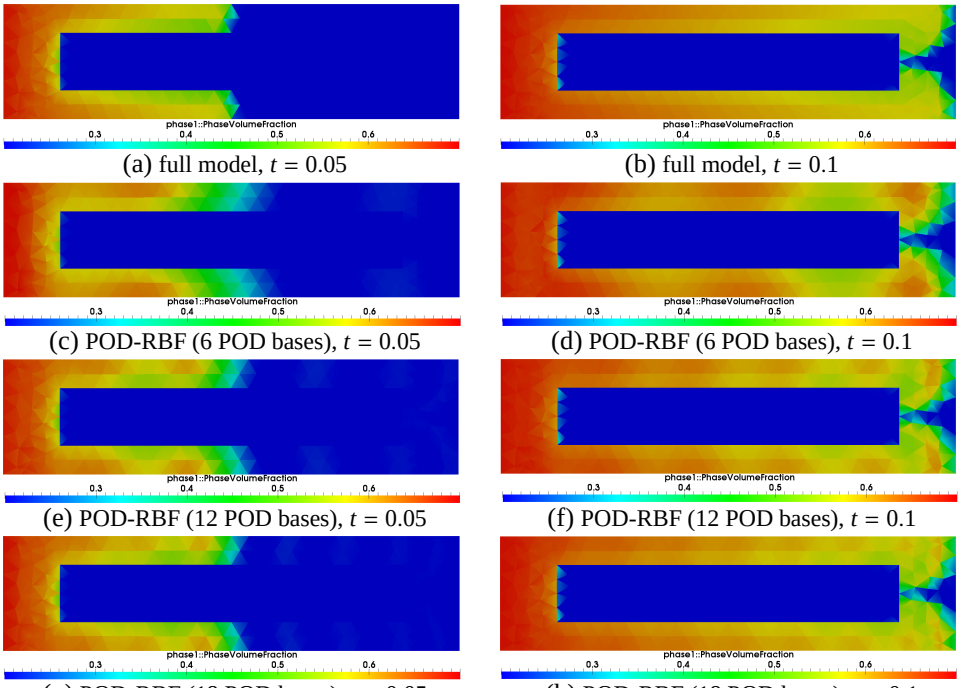

(a) full model, $t = 0.05$ (b) full model, $t = 0.1$

(c) POD-RBF (6 POD bases), $t = 0.05$ (d) POD-RBF (6 POD bases), $t = 0.1$

(e) POD-RBF (12 POD bases), $t = 0.05$ (f) POD-RBF (12 POD bases), $t = 0.1$

(g) POD-RBF (18 POD bases), $t = 0.05$ (h) POD-RBF (18 POD bases), $t = 0.1$

Figure 9: Case 2: the figures displayed above show the saturation solutions of the low permeability domain embedded in a higher permeability domain problem at time instances 0.05 and 0.1. The solutions compare the predictions from the non-intrusive POD-RBF model with full model using 6, 12 and 18 POD bases functions. The low permeability is 0.001 and the high permeability is 1.

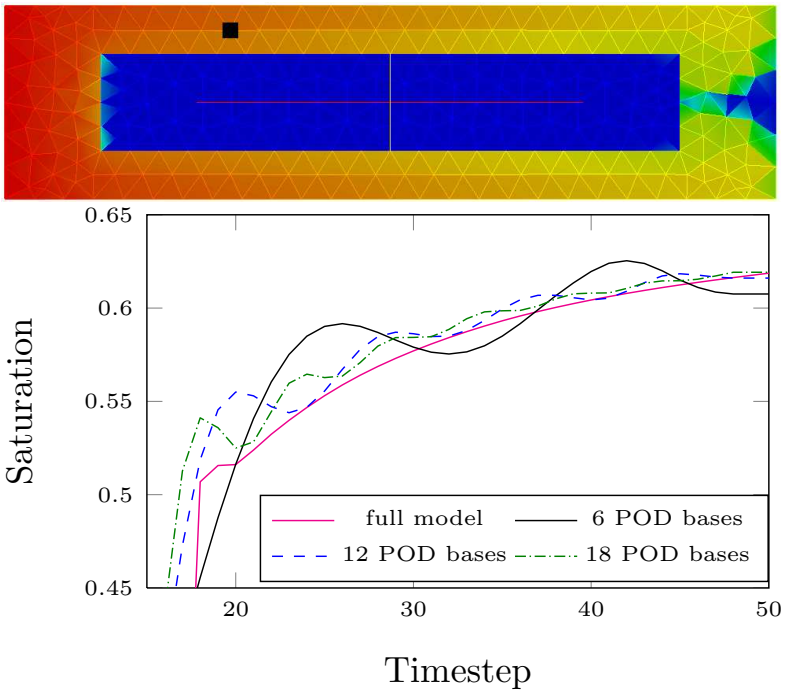

Figure 10: Case 2: the graph shows the solution saturations predicted by the full model and the POD-RBF ROM at a position: $x = 0.58515, y = 0.43611$ using 6, 12 and 18 POD bases.

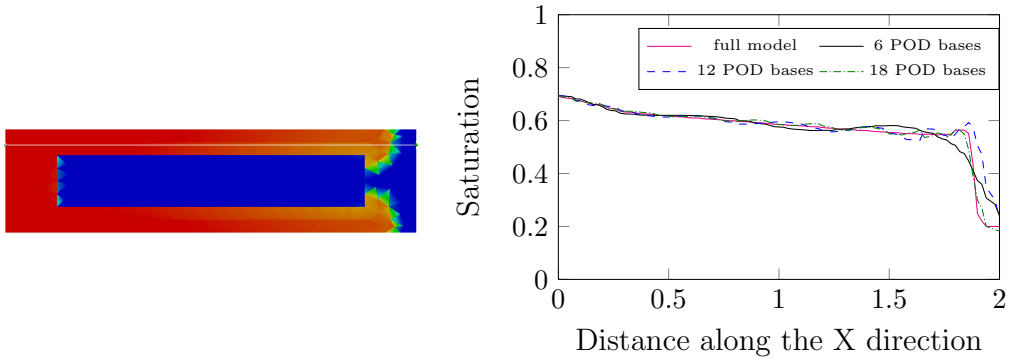

(a) The cross section location (b Saturation solution at the cross section

Figure 11: Case 2: Saturation along lines parallel to the x axies.

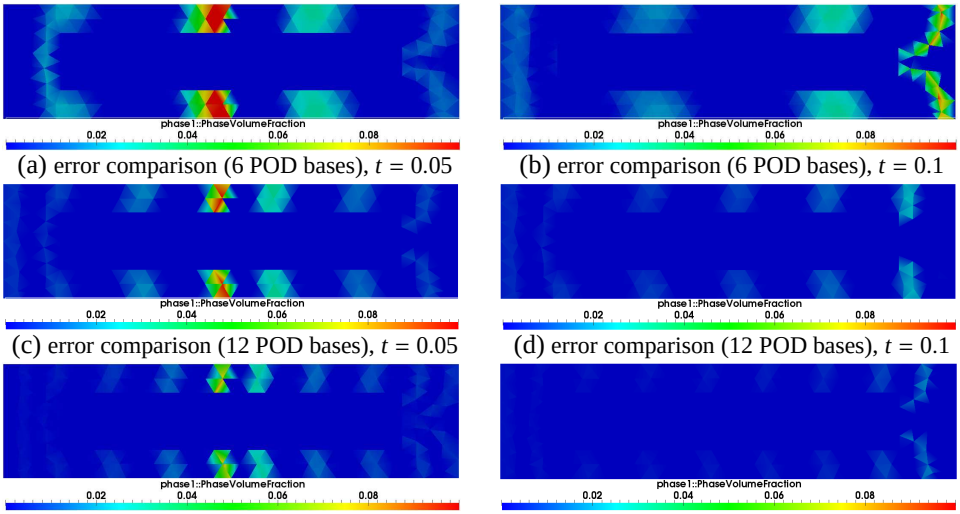

(a) error comparison (6 POD bases), $t = 0.05$ (b) error comparison (6 POD bases), $t = 0.1$

(c) error comparison (12 POD bases), $t = 0.05$ (d) error comparison (12 POD bases), $t = 0.1$

(e) error comparison (18 POD bases), $t = 0.05$ (f) error comparison (18 POD bases), $t = 0.1$

Figure 12: Case 2: the figures displayed above show the saturation error between full model and POD-RBF model of the low permeability domain embedded in a higher permeability domain problem at time instances 0.05 and 0.1 seconds using 6, 12 and 18 POD basis.

4.5. Efficiency of the POD-RBF model

Table 2 shows a comparison of the online CPU time required for running the full model and non-intrusive POD-RBF ROM. The simulations were performed on 12 cores machine of an Intel(R) Xeon(R) X5680 processor with 3.3GHz and 48GB RAM. The test cases were run in serial, which means only one core was used when simulating. Note that the offline CPU time required for constructing the POD bases and the interpolation function $f_{v,i,k}$, $f_{p,i,k}$ and $f_{S,i,k}$ (see algorithm 1) is not listed here. The online CPU time for running the POD-RBF model includes:

- interpolation for calculating the POD coefficients $v^n_{r,j}$, $p^n_{r,j}$ and $S^n_{r,j}$ (see equation (15));
- projecting the $v^n_{r,j}$, $p^n_{r,j}$ and $S^n_{r,j}$ onto the full space (see equation (7)).

It can be seen that the online CPU time required for running the POD-RBF model is considerably less than that for the full model and is reduced by a factor of 2500. It is worth noting that as the number of nodes increases the CPU time required for the full model increases rapidly while the CPU time for the POD-RBF model almost remains the same.

Table 2: Comparison of the online CPU time (dimensionless) required for running the full model and POD-RBF ROMs during one time step.

Cases	Model	assembling and solving	projection	interpolation	total
Case 1	Full model	0.81605	0	0	0.81605
	POD-RBF	0	0.0003	0.0001	0.00040
Case 2	Full model	1.15607	0	0	1.15607
	POD-RBF	0	0.0003	0.0001	0.00040

5. Conclusion

A non-intrusive POD reduced order model has been, for the first time, applied to porous media flows and developed for an advanced 3D unstructured mesh multiphase fluid model, the Imperial College Finite Element Reservoir Simulator (IC-FERST), which has the capabilities of using (1) anisotropic unstructured meshes to resolve fine scale flow feature; and (2) a novel control volume finite element method to resolve the high-order flux flows on CV boundaries. A RBF interpolation method is used to form a multi-dimensional interpolation function (hyper surface) that represents the solution of the multiphase porous media equations within the reduced space. The non-intrusive approach used here to construct the POD-RBF model is generic and does not require any information of the original source code or the model equations. It can be applied to any software or commercial codes. In addition, it avoids the instability of existing Galerkin POD ROMs, the results might be smoothed by RBF [46].

The capabilities of the newly developed POD-RBF multiphase porous media model are illustrated in two typical test cases in reservoir engineering. A comparison between

the full and POD-EBF model results are made. An error analysis was also carried out for the validation and accuracy assessment of the POD-RBF model. It is shown that the POD-RBF model exhibits an overall good agreement with the high fidelity full model. An increase in the number of POD bases leads to an improvement in the accuracy of the POD-RBF model. The saturation shock-front can be captured with relatively few POD basis functions, 18 POD basis function(figure (h) of 4) in the examples.

In comparison to the full model, without compromising the accuracy of results the CPU time required for the POD-RBF model can be reduced by a factor of 2500. It is worth of mentioning that for large scale porous media flow simulation, an increase in the number of nodes used in the computational domain will result in a large increase of the CPU time in the full simulation, but has very little effect on that of the POD-RBF model. Future work will investigate the effects of applying this new approach to more complex porous media flows.

Acknowledgment

This work was carried out under funding from the UK's Natural Environment Research Council (projects NER/A/S/2003/00595,NE/C52101X/1 and NE/C51829X/1), the Engineering and Physical Sciences Research Council (GR/R60898, EP/I00405X/1 and EP/J002011/1), and the Imperial College High Performance Computing Service. The authors would like to thank Pan Yang from AMCG, Imperial College London for helping to set up the test cases. Xiao acknowledges the support of china postdoctoral science foundation grant (2014M562087). Pain and Salinas would like to thanks EXXON for helping to fund the new unstructured mesh model used here; Pain and Fang are greatful for the support of BP on reduced order modelling under the LAMBSID project.

[1] D.T. Crommelin. and A.J. Majda. Strategies for model reduction: Comparing different optimal bases. *Journal of the Atmospheric Sciences*, 61:2206–2217, 2004.

[2] I.T. Jolliffe. Principal component analysis. *Springer, second edition*, pages 559–572, 2002.

[3] K. Fukunaga. Introduction to statistical recognition(2nd edn). *Computer Science and Scientific Computing Series*, Academic Press,Academic Press: Boston, MA.:5–33, 1990.

[4] K. Pearson. On lines and planes of closest fit to systems of points in space. *Philosophical Magazine*, 2:559–572, 1901.

[5] P.T.M. Vermeulen and A.W. Heemink. Model-reduced variational data assimilation. *Monthly Weather Review*, 134:2888–2899, 2006.

[6] D. Xiao, F. Fang, A. G. Buchan, C.C. Pain, I.M. Navon*, J. Du, , and G. Hu. Non-linear model reduction for the Navier-Stokes equations using Residual DEIM method. *Journal of Computational Physics*, 263:1–18, 2014.

[7] F.Fang, C.Pain, I.M. Navon, A.H. Elsheikh, J. Du, and D.Xiao. Non-linear Petrov-Galerkin methods for Reduced Order Hyperbolic Equations and Discontinuous Finite Element Methods. *Journal of Computational Physics*, 234:540–559, 2013.

[8] Y. Cao, J. Zhu, I.M. Navon, and Z. Luo. A reduced order approach to four dimensional variational data assimilation using proper orthogonal decomposition. *International Journal for Numerical Methods in Fluids*, 53:1571–1583, 2007.

[9] F Fang, T Zhang, D Pavlidis, C.C. Pain, AG Buchan, and I.M. Navon. Reduced order modelling of an unstructured mesh air pollution model and application in 2d/3d urban street canyons. *Atmospheric Environment*, 96:96–106, 2014.

[10] F Fang, C.C. Pain, I.M. Navon, GJ Gorman, MD Piggott, PA Allison, and AJH Goddard. A POD goal-oriented error measure for mesh optimization. *International Journal for Numerical Methods in Fluids*, 63(2):185–206, 2010.

[11] Razvan Stefanescu and I.M. Navon. POD/DEIM nonlinear model order reduction of an adi implicit shallow water equations model. *Journal of Computational Physics*, 237:95–114, 2013.

[12] Razvan Stefanescu, Adrian Sandu, and I.M. Navon. Comparison of POD reduced order strategies for the nonlinear 2D shallow water equations. *International Journal for Numerical Methods in Fluids*, 76(8):497–521, 2014.

[13] D.N. Daescu and I.M. Navon. A dual-weighted approach to order reduction in 4d-var data assimilation. *Monthly Weather Review*, 136(3):1026–1041, 2008.

[14] Muhammad Umer Altaf. *Model Reduced Variational Data Assimilation for Shallow Water Flow Models*. PhD thesis, Delft University of Technology, 2011.

[15] X. Chen, I.M. Navon, and F. Fang. A dual-weighted trust-region adaptive POD 4D-VAR applied to a finite-element shallow-water equations model. *International Journal for Numerical Methods in Fluids*, 65(5):520–541, 2011.

[16] X. Chen, S. Akella, and I.M. Navon. A dual-weighted trust-region adaptive POD 4-D var applied to a finite-volume shallow water equations model on the sphere. *International Journal for Numerical Methods in Fluids*, 68(3):377–402, 2012.

[17] J. Du, F. Fang, C.C. Pain, I.M. Navon, J. Zhu, and D.A. Ham. POD reduced-order unstructured mesh modeling applied to 2D and 3D fluid flow. *Computers and Mathematics with Applications*, 65:362–379, 2013.

[18] Leopoldo P. Franca and Sergio L. Frey. Stabilized finite element methods: Ii. the incompressible Navier-Stokes equations. *Computer Methods in Applied Mechanics and Engineering*, 99(2-3):209–233, 1992.

[19] D. Xiao, F. Fang, J. Du, C.C. Pain, I.M. Navon, A. G. Buchan, A.H. ElSheikh, and G. Hu. Non-linear Petrov-Galerkin methods for reduced order modelling of the Navier-Stokes equations using a mixed finite element pair. *Computer Methods In Applied Mechanics and Engineering*, 255:147–157, 2013.

[20] Alireza Jafarpour Feriedoun Sabetghadam. α Regularization of the POD-Galerkin dynamical systems of the Kuramoto-Sivashinsky equation. *Applied Mathematics and Computation*, 218:6012–6026, 2012.

[21] C. Bou-Mosleh K. Carlberg and C. Farhat. Efficient non-linear model reduction via a least-squares Petrov-Galerkin projection and compressive tensor approximations. *International Journal for Numerical Methods in Engineering*, 86:155–181, 2011.

[22] M. Serpas Y. Chu and J. Hahn. State-preserving nonlinear model reduction procedure. *Chemical Engineering Science*, 66:3907–3913, 2011.

[23] Karen Willcox and Alexandre Megretski. Model reduction for large-scale linear applications. In *Proc. of 13th IFAC Symposium on System Identification, Rotterdam, Netherlands*, pages 1431–1436, 2003.

[24] M. Barrault, Y. Maday, N.C. Nguyen, and A.T. Patera. An empirical interpolation method: application to efficient reduced-basis discretization of partial differential equations. *C. R. Acad. Sci. Paris, Ser*, 339:667–672, 2004.

[25] S. Chaturantabut and D.C. Sorensen. Nonlinear model reduction via discrete empirical interpolation. *SIAM J. Sci. Comput*, 32:2737–2764, 2010.

[26] Kevin Carlberg, Charbel Farhat, Julien Cortial, and David Amsallem. The gnat method for nonlinear model reduction: effective implementation and application to computational fluid dynamics and turbulent flows. *Journal of Computational Physics*, 242:623–647, 2013.

[27] Juan Du, Fangxin Fang, Christopher C Pain, I.M. Navon, Jiang Zhu, and David A Ham. POD reduced-order unstructured mesh modeling applied to 2d and 3d fluid flow. *Computers and Mathematics with Applications*, 65(3):362–379, 2013.

[28] F Fang, CC Pain, I.M. Navon, MD Piggott, GJ Gorman, PA Allison, and AJH Goddard. Reduced-order modelling of an adaptive mesh ocean model. *International journal for numerical methods in fluids*, 59(8):827–851, 2009.

[29] Chen Han. Blackbox stencil interpolation method for model reduction. Master's thesis, Massachusetts Institute of Technology, 2012.

[30] Christophe Audouze, Florian De Vuyst, and Prasanth B Nair. Nonintrusive reduced-order modeling of parametrized time-dependent partial differential equations. *Numerical Methods for Partial Differential Equations*, 29(5):1587–1628, 2013.

[31] C Audouze, F De Vuyst, and PB Nair. Reduced-order modeling of parameterized pdes using time–space-parameter principal component analysis. *International journal for numerical methods in engineering*, 80(8):1025–1057, 2009.

[32] S Walton, O Hassan, and K Morgan. Reduced order modelling for unsteady fluid flow using proper orthogonal decomposition and radial basis functions. *Applied Mathematical Modelling*, 37(20):8930–8945, 2013.

[33] T Heijn, R Markovinovic, Jansen, and J-D. Generation of low-order reservoir models using system-theoretical concepts. *SPE Journal*, 9(02):202–218, 2004.

[34] Marco Antonio Cardoso. *Development and application of reduced-order modeling procedures for reservoir simulation*. ProQuest, 2009.

[35] MA Cardoso, LJ Durlofsky, and P Sarma. Development and application of reduced-order modeling procedures for subsurface flow simulation. *International journal for numerical methods in engineering*, 77(9):1322–1350, 2009.

[36] Saifon Chaturantabut and Danny C Sorensen. Application of POD and DEIM on dimension reduction of non-linear miscible viscous fingering in porous media. *Mathematical and Computer Modelling of Dynamical Systems*, 17(4):337–353, 2011.

[37] Yanfang Yang, Yalchin Efendiev, Mohammadreza Ghasemi, Eduardo Gildin, Victor Manuel Calo, et al. Fast multiscale reservoir simulations using pod-deim model reduction. In *SPE Reservoir Simulation Symposium*. Society of Petroleum Engineers, 2015.

[38] Seonkyoo Yoon, Zeid Alghareeb, John Williams, et al. Development of reduced-order oil reservoir models using localized deim. In *SPE Annual Technical Conference and Exhibition*. Society of Petroleum Engineers, 2014.

[39] Mohammadreza Ghasemi, Ashraf Ibrahim, Eduardo Gildin, et al. Reduced order modeling in reservoir simulation using the bilinear approximation techniques. In *SPE Latin America and Caribbean Petroleum Engineering Conference*. Society of Petroleum Engineers, 2014.

[40] Hector Klie et al. Unlocking fast reservoir predictions via nonintrusive reduced-order models. In *SPE Reservoir Simulation Symposium*. Society of Petroleum Engineers, 2013.

[41] Ahmad Jan Khattak, SIA Tirmizi, et al. Application of meshfree collocation method to a class of nonlinear partial differential equations. *Engineering analysis with boundary elements*, 33(5):661–667, 2009.

[42] Mehdi Dehghan and Ali Shokri. A meshless method for numerical solution of the one-dimensional wave equation with an integral condition using radial basis functions. *Numerical Algorithms*, 52(3):461–477, 2009.

[43] Michael JD. Powell. The theory of radial basis function approximation in 1990. *Advances in numerical analysis 2*, pages 105–210, 1992.

[44] P. Salinas, J. R. Percival, D. Pavlidis, Z. Xie, J. Gomes, C. C. Pain, and M. D. Jackson. A discontinuous overlapping control volume finite element method for multi-phase porous media flow using dynamic unstructured mesh optimization. In *SPE 173279*, 2015.

[45] Kai Su, J-P Latham, Dimitrios Pavlidis, Jiansheng Xiang, Fangxin Fang, Peyman Mostaghimi, James R Percival, Christopher C Pain, and Matthew D Jackson. Multiphase flow simulation through porous media with explicitly resolved fractures. *Geofluids*, 2015.

[46] Donald E Myers. Smoothing and interpolation with radial basis functions. *BOUNDARY ELEMENT TECHNOLOGY*, 13:365–376, 1999.